Supporting Information of

Optimising broadband pulses for DEER depends on concentration and distance range of interest

Andreas Scherer, Sonja Tischlik, Sabrina Weickert, Valentin Wittmann, Malte Drescher

Department of Chemistry and Konstanz Research School Chemical Biology, University of Konstanz, Konstanz, Germany

Correspondence to: Malte Drescher (malte.drescher@uni–konstanz.de)

Contents

S1 Additional materials and methods

All experiments have been performed on a Bruker Elexsys E580 spectrometer at Q-band (34 GHz). The spectrometer is equipped with a SpinJet-AWG unit (Bruker) and a 150 W pulsed travelling-wave tube (TWT) amplifier (Applied Systems Engineering, Fort Worth, USA). All samples were measured in 3 mm outer diameter sample tubes in an overcoupled ER5106QT-2 resonator (Bruker). The quality factor Q of the overcoupled resonator is approximately 200.

The samples were cooled to 50 K with a Flexline helium recirculation system (CE-FLEX-4K-0110, Bruker Biospin, ColdEdge Technologies) comprising a cold head (expander, SRDK-408D2) and a F-70H compressor (both SHI cryogenics, Tokyo, Japan), controlled by an Oxford Instruments Mercury ITC.

S1.1 EDFS

The echo-detected-field sweep spectra were recorded with a Hahn echo sequence ($\frac{\pi}{2}$ - τ - π - $\tau -$ echo) pulse-sequence with $\tau = 1.5$ µs, a sweep width of 200 G and 10 shots per point, 3 scans and rectangular pulses. The length of the π-pulse was 16 ns at a frequency of 34 GHz.

S1.2 Nutation experiments

Pulse lengths of rectangular and Gaussian pulses were determined with nutation experiments with the pulse sequence (inversion pulse $- \tau_1 - \frac{\pi}{2} - \tau_2 - \pi - \tau_2 -$ echo). τ_1 was set to 1 µs.

S1.3 Resonator profile

The resonator profile was measured by a series of nutation experiments at different frequencies as described in the literature (Doll and Jeschke, 2014). It was measured over 300 MHz with a step size of 10 MHz. The magnetic field was co-stepped. The nutation frequencies were calculated by a Fourier transformation of the nutation traces.

S1.4 DEER

All DEER experiments were measured with the standard four pulse DEER sequence:

$$\frac{\pi}{2}_{obs} - \tau_1 - \pi_{\mathrm{obs}} - t - \pi_{\mathrm{pump}} - \tau_1 + \tau_2 - t - \pi_{\mathrm{obs}} - \tau_2 - \mathrm{echo}$$

The delay between the $\pi/2$ and the π pulse in the observer channel τ_1 was 400 ns. The dipolar evolution time τ_2 was 8 µs. For all DEER experiments with rectangular and Gaussian pump pulses the pump frequency was set to 34.00 GHz. The magnetic field was chosen such that the pump lies on the maximum of the nitroxide spectrum. We used the phase cycling ((x) [x] x_p x) as suggested by (Tait and Stoll, 2016) and nuclear modulation averaging as suggested by (Jeschke, 2012).

S1.5 DEER optimisation

For the optimisation measurements we used a python script that can automatically perform several DEER experiments after another. We shifted the magnetic field from 1.2090 T to 1.2113 T for an observer pulse of 33.91 GHz and from 1.2097 T to 1.2119 T for an observer position of 33.93 GHz to ensure that the pump pulse is on the maximum of the nitroxide spectrum. Figure S1 illustrates the idea with a fixed observer frequency of 33.93 GHz.

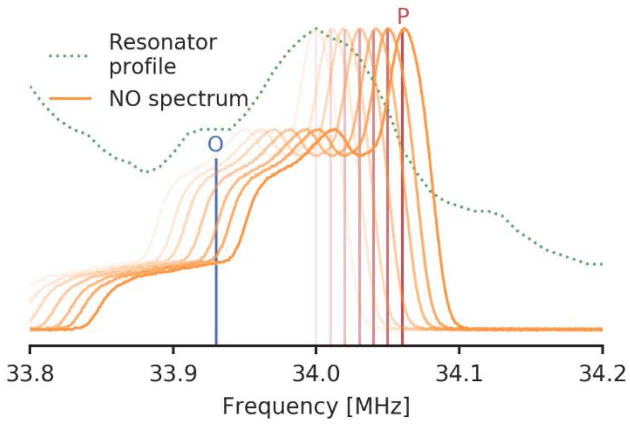

Figure S1: The resonator profile (green dots) with the different offsets during an optimisation measurement. The nitroxide spectrum (orange) is shifted with the offset. The observer frequency stays fixed at 33.93 GHz and is indicated by a blue line. The shift of the pump spin is indicated by the red line.

S1.6 Pulse calculations

For rectangular and Gaussian pulses, we used the pulses that are generated by Bruker Xepr software. For Gaussian pulses the FWHM is defined by FWHM $= \frac{t_{\mathrm{p}}}{2\sqrt{2\ln(2)}}$. All other pulses were calculated with the *pulse* function from the *easyspin* (Version 5.2.21) package for MATLAB R2018b (Stoll and Schweiger, 2006). The resulting pulse shapes were normalised to amplitude values between -1 and 1 and loaded into Xepr.

S1.7 Integration window

The integration window was determined by recording a series of 300 Hahn echoes in transient mode. We evaluated the signal-to-noise (SNR) with different integration windows and determined the integration window with the maximum SNR.

S2 Determination of the integration window

To determine the ideal integration window we recorded a series of Hahn echoes and calculated the SNR ratio for different integration window lengths. The results show that for rectangular pulses the ideal integration window is typically longer than the π-pulse length (Fig. S2). An improvement of up to 14 % for a π-pulse length of 28 ns and an ideal integration window of 44 ns was achieved.

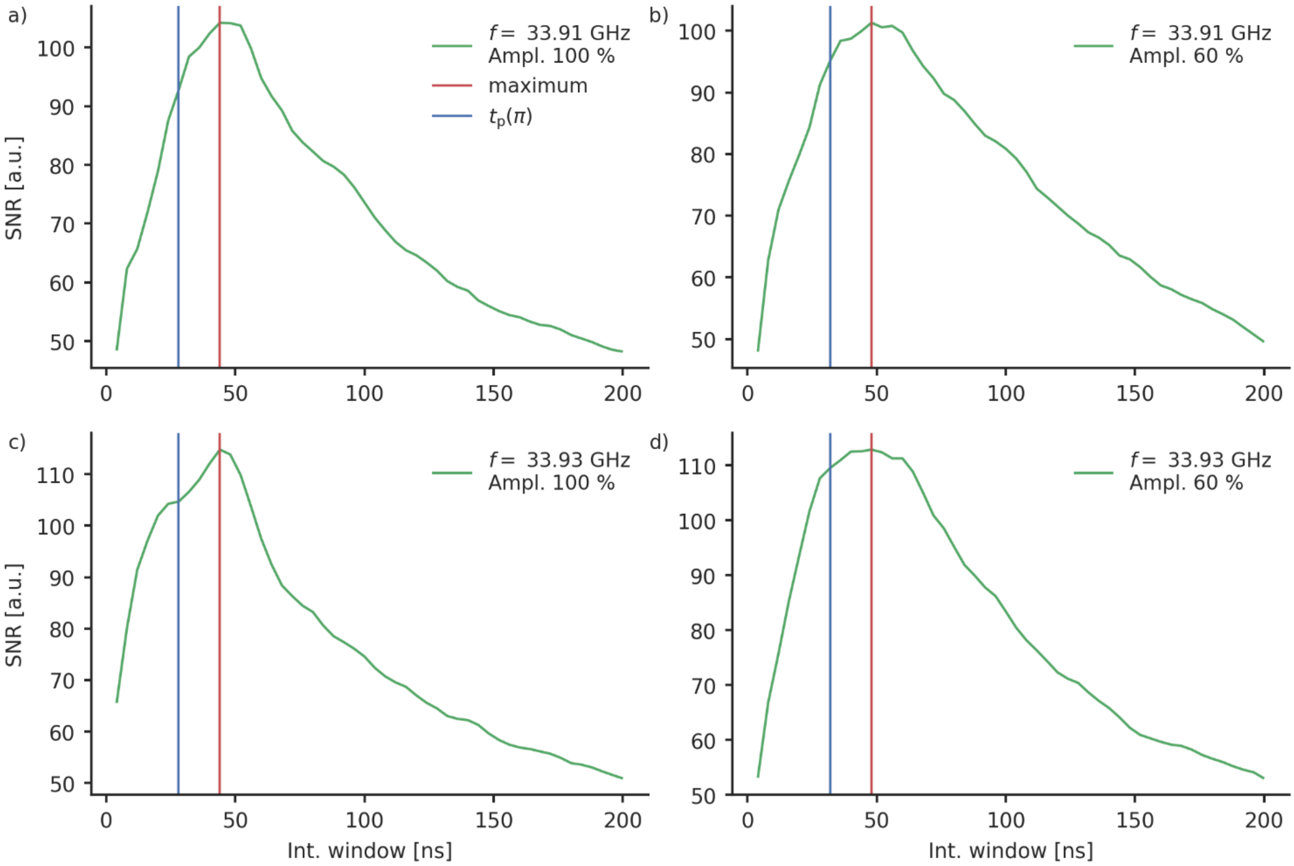

Figure S2: The SNR for rectangular pulses of a series of transient Hahn echoes is shown as a function of the integration window length. The red lines indicate the integration window with the maximum SNR, the blue lines indicate an integration window that has the length of the π-pulse. The pulses have the following settings: a) frequency: 33.91 GHz, amplitude: 100 %. b) frequency: 33.91 GHz, amplitude: 60 %. c) frequency: 33.93 GHz, amplitude: 100 %. d) frequency: 33.93 GHz, amplitude: 60 %.

For Gaussian pulses the ideal integration window is typically smaller than the π-pulse length (figure S3).

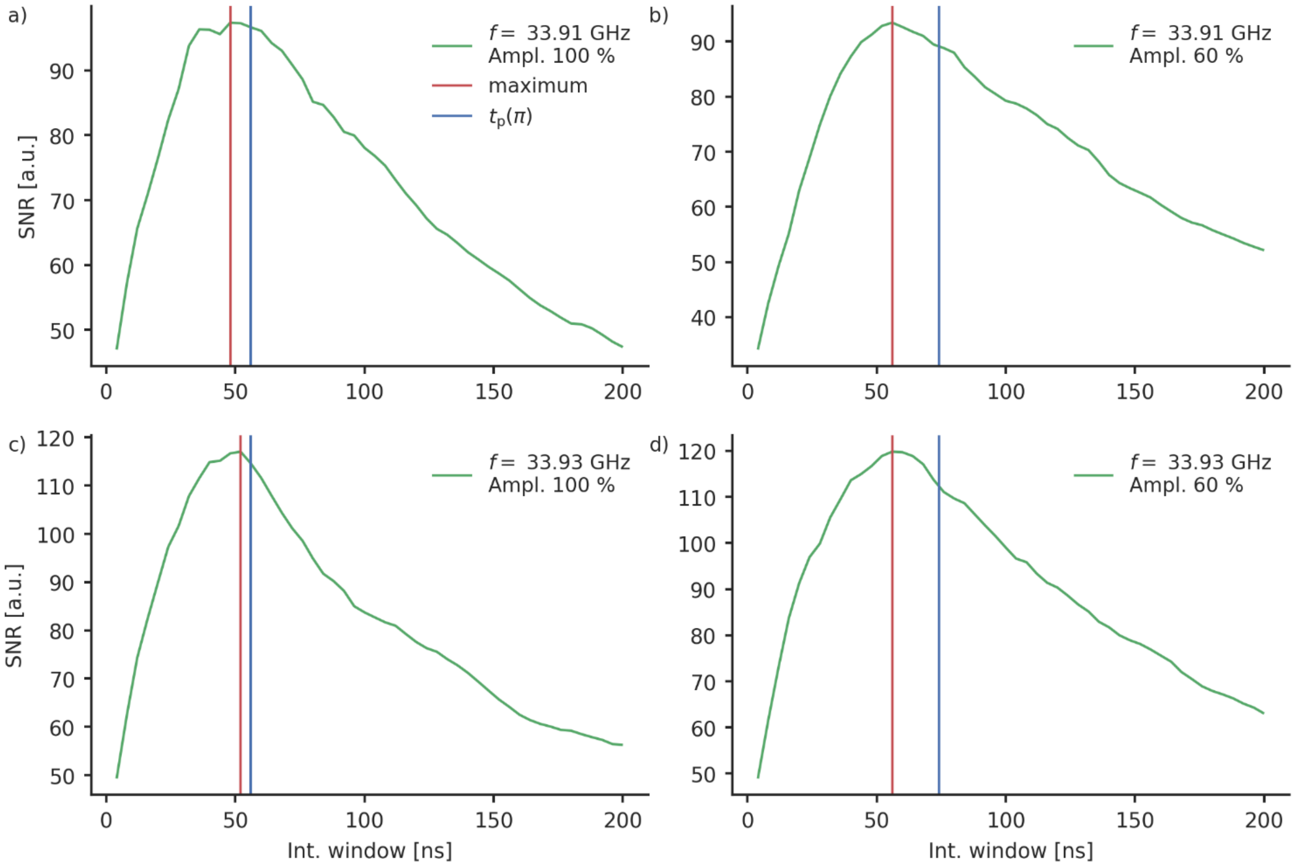

Figure S3: The SNR for Gaussian pulses of a series of transient Hahn echoes is shown as a function of the integration window length. The red lines indicate the integration window with the maximum SNR, the blue lines indicate an integration window that has the length of the π-pulse. The pulses have the following settings: a) frequency: 33.91 GHz, amplitude: 100 %. b) frequency: 33.91 GHz, amplitude: 60 %. c) frequency: 33.93 GHz, amplitude: 100 %. d) frequency: 33.93 GHz, amplitude: 60 %.

S3 Parameters for the observer pulse

Table S1: Parameters for the rectangular observer pulses. The pulse length is referring to the π-pulse.

f_{obs} [GHz]	Obs. Amp. [%]	t_π [ns]	Length of integration window [ns]
33.91	100	28	44
	60	32	48
33.93	100	28	44
	60	32	48

Table S2: Parameters for the Gaussian observer pulses. The pulse length is referring to the π-pulse.

f_{obs} [GHz]	Obs. Amp. [%]	t_π [ns]	Length of integration window [ns]
33.91	100	56	48
	60	74	56
33.93	100	56	52
	60	74	56

S4 The MNR for rectangular and Gaussian pump pulses evaluated up to 7 µs

Table S3: MNR for a rectangular pump pulse and different rectangular observer pulses. The pump pulses had a length of 16 ns. The MNR has been evaluated up to 7 µs.

f_{obs} [GHz]	Obs. Amp. [%]	t_π [ns]	MNR	Mod depth λ
33.91	100	28	30	0.32
	60	32	32	0.32
33.93	100	28	32	0.31
	60	32	35	0.31

Table S4: MNR for a Gaussian pump pulse and different Gaussian observer pulses. The pump pulses had a length of 34 ns. The MNR has been evaluated up to 7 µs.

f_{obs} [GHz]	Obs. Amp. [%]	t_π [ns]	MNR	Mod depth λ
33.91	100	56	36	0.31
	60	74	32	0.29
33.93	100	56	41	0.31
	60	74	38	0.31

S5 Inversion profiles for rectangular and Gaussian pulses

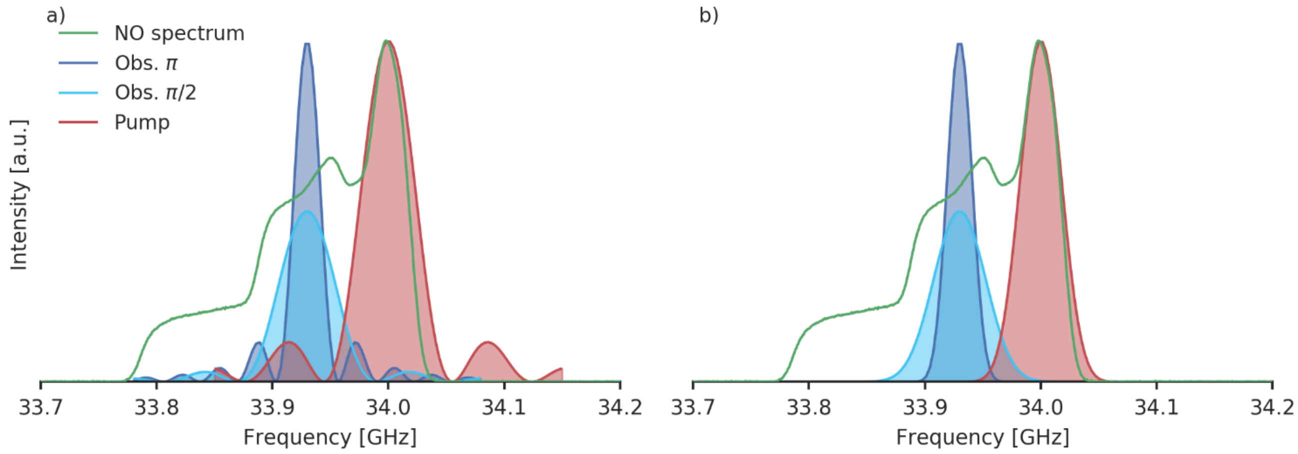

Figure S4: The excitation profiles of the observer (blue) and pump pulses (red) of (a) rectangular and (b) Gaussian pulses. The light blue profiles are for the $\pi/2$ observer pulses and the dark blue profiles for the π observer pulse. The rectangular observer pulses have an amplitude of 60 %, a pulse length of 32 ns (π on observer) and 16 ns (pump), and the Gaussian have an amplitude of 100 %, a length of 56 ns (π on observer) and 34 ns (pump). It can be seen that the spectral overlap can be reduced with Gaussian pulses. The pulse amplitudes of the pump pulse are always 100 %.

S6 Simulations of spin inversion trajectories

We simulated the effect of an HS{1,1} pulse with a pulse length of 100 ns, a truncation parameter of $\beta = 8/t_p$, a frequency sweep range from -55 MHz and 55 MHz. We performed the numerical simulation in the density operator framework with MATLAB R2018b. The maximum of the B_1-field was set to 30 MHz, which corresponds to the maximum of the resonator profile. This pulse shows a good inversion between a frequency range of -40 MHz and 40 MHz (figure S7a). In figure S7b, the inversion of a spin packet with an offset of -40 MHz and 40 MHz are shown. It can be seen that the spins are inverted in a time window between 20 ns and 80 ns, making an effective pulse length of 60 ns. This corresponds to a minimum distance of 2.32 nm.

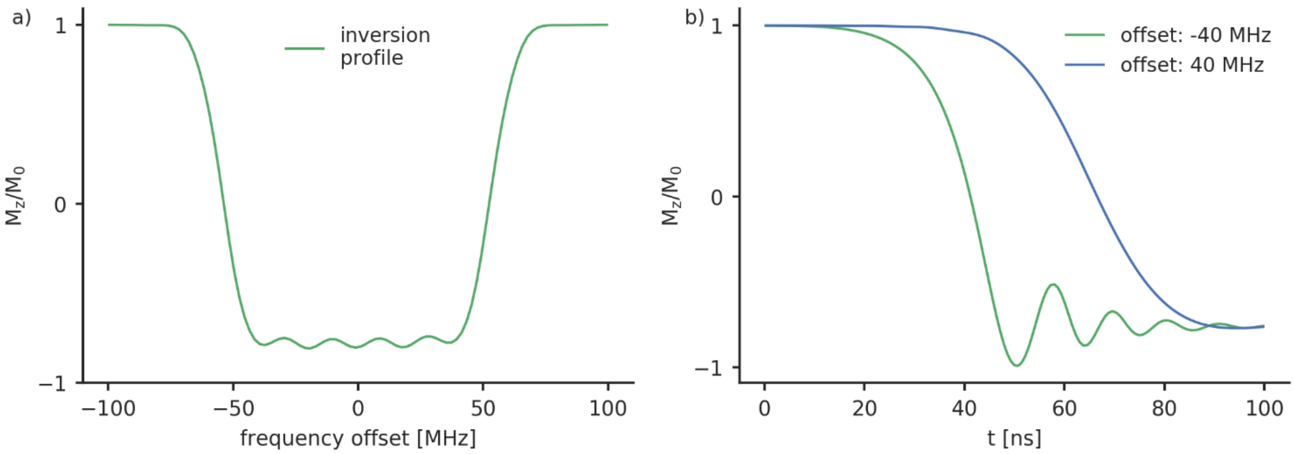

Figure S5: a) The excitation profile of HS{1,1} with a pulse length of 100 ns, a truncation of $\beta = 8/t_p$ and a frequency range from -55 MHz and +55 MHz. b) The inversion of a spin packet with an offset of -40 MHz (blue) and +40 MHz (green).

S7 The MNR for broadband pump pulses evaluated up to 7 µs

Table S5: MNR for the different broadband shaped pulses with a rectangular observer pulse. The MNR has been evaluated up to 7 µs.

f_{obs} [GHz]	Obs. Amp. [%]	Pump pulse	t_π [ns]	Δf [MHz]	Offset [MHz]	MNR	Mod. depth λ
33.91	100	HS{1,6} ($\beta = 8/t_p$)	100	110	90	32	0.63
		WURST (n=6)	100	160	90	37	0.64
		Chirp ($t_r = 30$ ns)	36	120	90	33	0.50
		HS{1,1} ($\beta = 6/t_p$)	100	110	90	41	0.57
	60	HS{1,6} ($\beta = 10/t_p$)	100	110	90	31	0.62
		WURST (n=6)	100	160	90	30	0.64
		Chirp ($t_r = 30$ ns)	100	160	90	32	0.67
		HS{1,1} ($\beta = 6/t_p$)	100	110	90	34	0.57
33.93	100	HS{1,6} ($\beta = 10/t_p$)	100	110	100	39	0.57
		WURST (n=6)	100	160	100	39	0.62
		Chirp ($t_r = 10$ ns)	36	120	90	38	0.47
		HS{1,1} ($\beta = 6/t_p$)	100	110	90	43	0.53
	60	HS{1,6} ($\beta = 10/t_p$)	100	110	90	40	0.60
		WURST (n=6)	100	120	100	36	0.57
		Chirp ($t_r = 10$ ns)	36	120	90	38	0.47
		HS{1,1} ($\beta = 8/t_p$)	100	90	80	43	0.48

Table S6: MNR for the different broadband shaped pulses with a Gaussian observer pulse. The MNR has been evaluated up to 7 μs.

f_{obs} [GHz]	Obs. Amp. [%]	Pump pulse	t_{π} [ns]	Δf [MHz]	Offset [MHz]	MNR	Mod. depth λ
33.91	100	HS{1,6} ($\beta = 10/t_p$)	100	90	90	36	0.60
		WURST (n=6)	100	160	90	30	0.64
		Chirp ($t_r = 10$ ns)	36	120	80	37	0.50
		HS{1,1} ($\beta = 6/t_p$)	100	110	90	40	0.58
	60	HS{1,6} ($\beta = 8/t_p$)	100	110	90	38	0.63
		WURST (n=6)	100	160	100	34	0.48
		Chirp ($t_r = 10$ ns)	100	120	90	38	0.48
		HS{1,1} ($\beta = 6/t_p$)	100	110	90	37	0.58
33.93	100	HS{1,6} ($\beta = 10/t_p$)	100	90	90	39	0.57
		WURST (n=6)	100	160	100	38	0.62
		Chirp (no smoothing)	36	120	80	45	0.49
		HS{1,1} ($\beta = 8/t_p$)	100	110	90	50	0.52
	60	HS{1,6} ($\beta = 10/t_p$)	100	110	90	45	0.61
		WURST (n=6)	100	160	90	40	0.63
		Chirp ($t_r = 9$ ns)	36	120	80	45	0.47
		HS{1,6} ($\beta = 8/t_p$)	100	110	80	47	0.52

S8 Inversion profiles for the broadband shaped pulses

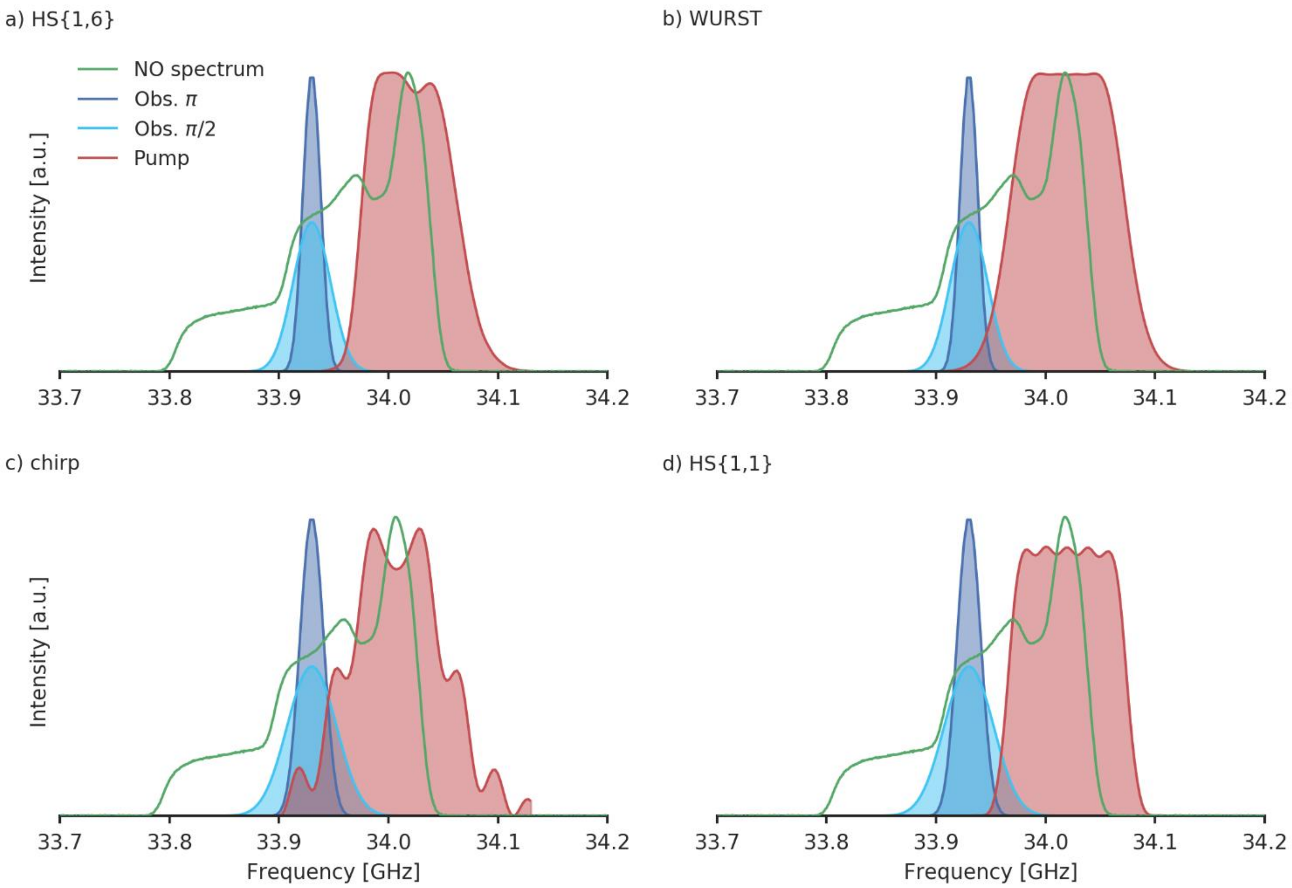

Figure S6: The inversion profiles of a (a) HS{1,6}, (b) WURST, (c) chirp and (d) HS{1,1} pulse. The parameters of the pump and observer pulses can be found in table 2 of the main text.

S9 Pulse shaped of the broadband shaped pulses

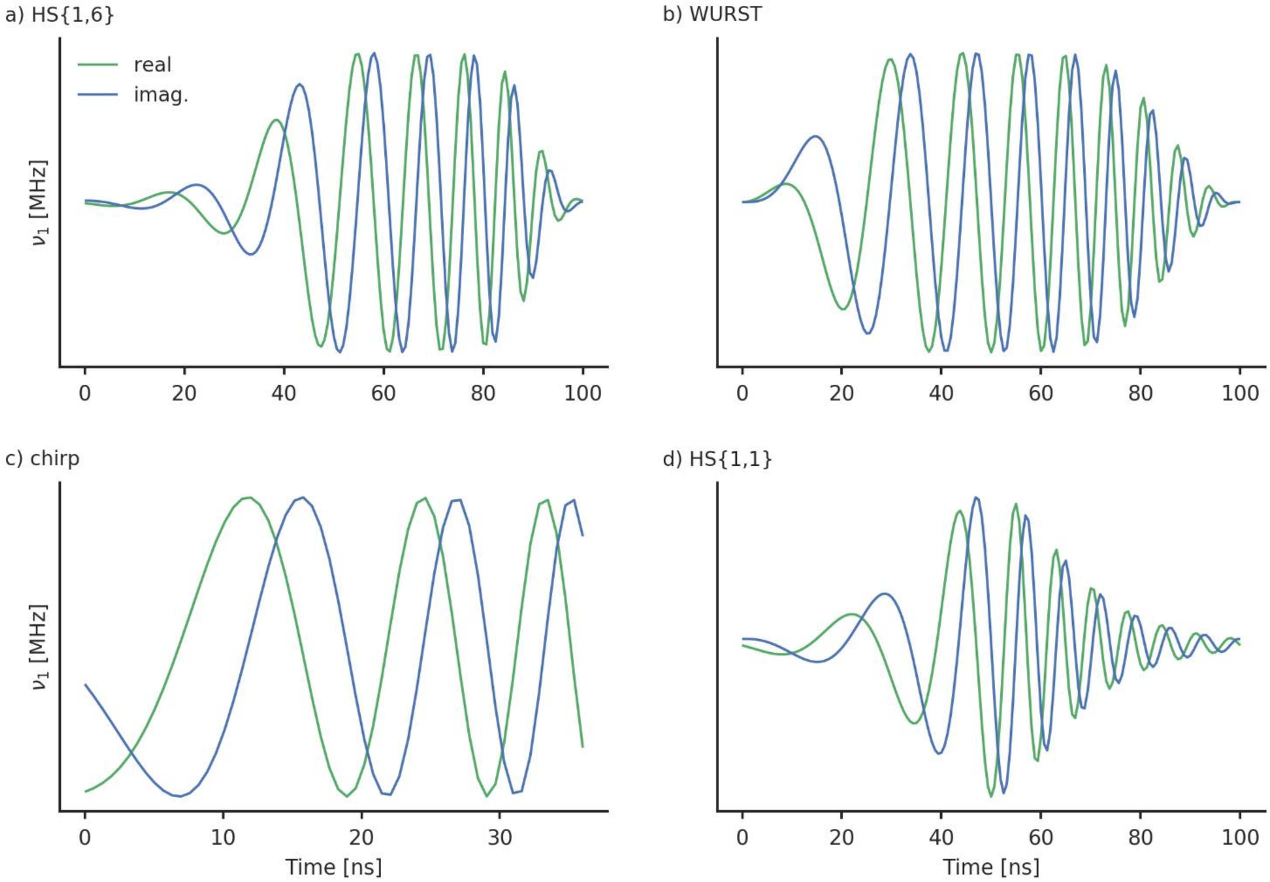

Figure S7: The pulse shaped of an (a) HS{1,6} , (b) WURST , (c) chirp and (d) HS{1,1} pulse with the real part (green) and imaginary part (blue). The parameters broadband shaped pulses can be found in table 2 of the main text.

S10 Comparison of full DEER traces

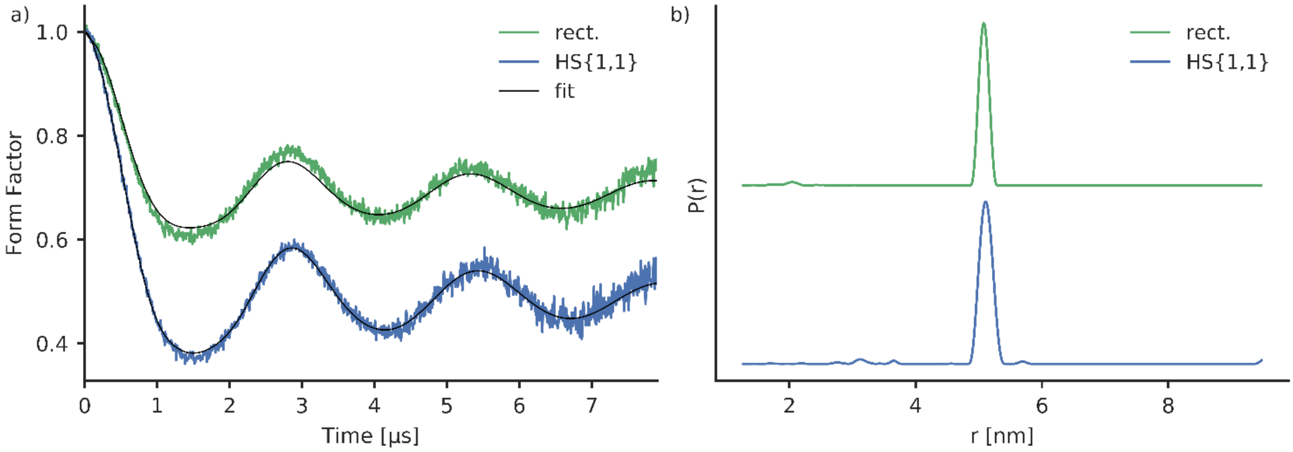

Figure S8: Comparison of the performance of DEER with rectangular pulses (green) and with Gaussian observer pulses and the HS{1,1} pulse from table 1 that yielded the best MNR (blue). The form factors are shown in (a) and the corresponding distance distributions in (b). One 10 minute scan was recorded for both experiments.

S11 Comparison of bandwidth compensated and non-bandwidth compensated pulses

We tested the performance of a bandwidth compensation for HS{1,6}, WURST, chirp and HS{1,1} pump pulses. The observer pulses were rectangular with an offset of 90 MHz and an observer π pulse length of 28 ns. We estimated the effect of bandwidth compensation with the help of the $\eta_{2\mathrm{p}}$ parameter. For WURST and chirp pulses, a bandwidth compensation lead to an improvement of 3.0 % and 3.2 %. However, for HS{1,6} and HS{1,1} pulses, we observed a decrease of 10.5% and 2.6% (data not shown). As a bandwidth compensation requires a measurement of the resonator profile before each DEER measurement and did not always result in an increase in performance, we decided to stick to pulses without bandwidth compensation.

S12 Comparison of 100 ns and 200 ns pulse lengths

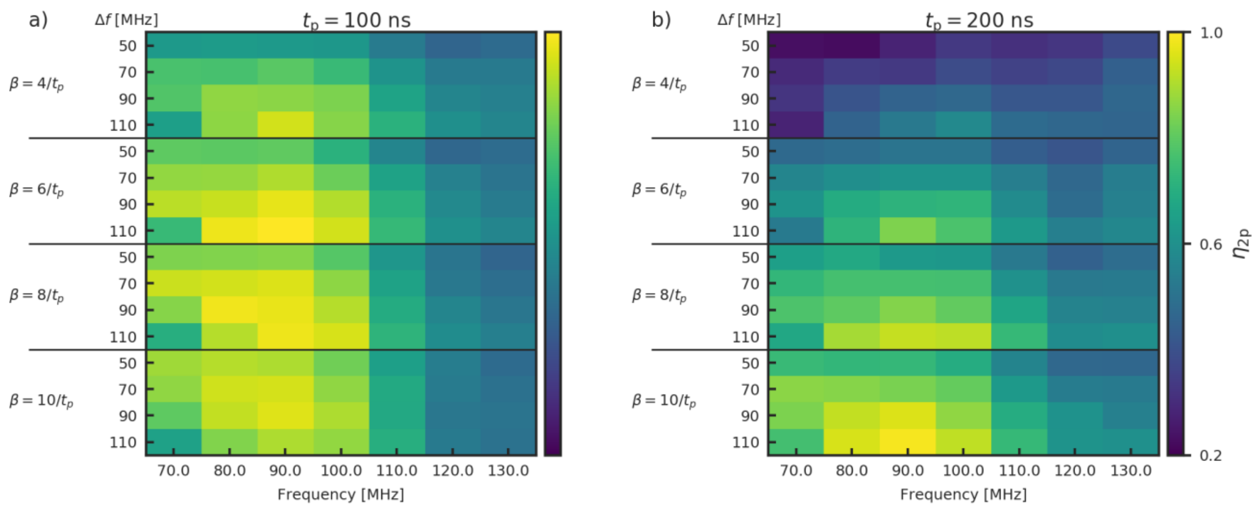

Figure S9: HS{1,1} pump pulses of (a) 100 ns and (b) 200 ns length. The observer pulses were rectangular with 100 % intensity at an observer position of 33.91 GHz and a pulse length of 28 ns for the π pulse.

S13 Echo decrease with long broadband shaped pump pulses

We have checked the echo intensity at the zero time of the DEER trace with different pump pulses. There is always a slight decrease of the echo intensity in the presence of a pump pulse (Fig. S8a). It is, however, negligible for rectangular pump pulses. With a 100 ns HS{1,1} pulse there is a stronger decrease of the echo, which gets even worse for 200 ns and 400 ns pulses. In the last case, nearly the whole echo has disappeared. The reason for this behaviour is not entirely clear to us as the excitation profiles do not change significantly with the pulse length (Fig. S8 b). However, we chose not to investigate 200 ns and 400 ns pulses.

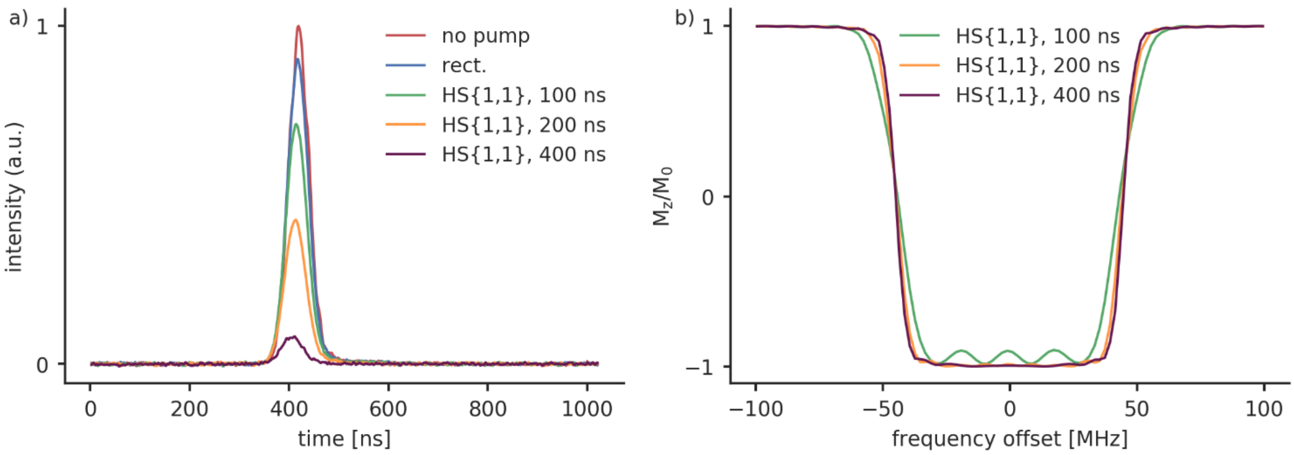

Figure S10: a) The echoes are at the zero time of the DEER trace. The echoes are recorded without a pump pulse (red), with a rectangular pump pulse (blue), with a 100 ns (green), 200 ns (yellow) and 400 ns (purple) HS{1,1} pump pulse (b) shows the excitation profile of the respective HS{1,1} pump pulses. Their parameters are $\beta = 6/t_p$, $\Delta f = 90$ MHz, offset to observer: 80 MHz and a pulse length of 100 ns (green), 200 ns (yellow) and 400 ns (purple).

S14 The MNR for rectangular and Gaussian pump pulses evaluated up to 2 μs

Table S7: MNR for a rectangular pump pulse and different rectangular observer pulses. The pump pulses had a length of 16 ns. The MNR has been evaluated up to 2 μs.

f_{obs} [GHz]	Obs. Amp. [%]	t_{π} [ns]	MNR	Mod. depth λ
33.91	100	28	41	0.32
	60	32	41	0.32
33.93	100	28	40	0.31
	60	32	44	0.31

Table S8: MNR for a Gaussian pump pulse and different Gaussian observer pulses. The pump pulses had a length of 34 ns. The MNR has been evaluated up to 2 μs.

f_{obs} [GHz]	Obs. Amp. [%]	t_{π} [ns]	MNR	Mod. depth λ
33.91	100	56	50	0.31
	60	74	42	0.29
33.93	100	56	53	0.31
	60	74	48	0.31

S15 The MNR for broadband pump pulses evaluated up to 2 μs

Table S9: MNR for the different broadband shaped pulses with a rectangular observer pulse. The MNR has been evaluated up to 2 μs.

f_{obs} [GHz]	Obs. Amp. [%]	Pump pulse	t_π [ns]	Δf [MHz]	Offset [MHz]	MNR	Mod. depth λ
33.91	100	HS{1,6} ($\beta = 8/t_p$)	100	110	90	58	0.63
		WURST (n=6)	100	160	90	60	0.64
		Chirp ($t_r = 30$ ns)	36	120	90	52	0.50
		HS{1,1} ($\beta = 6/t_p$)	100	110	90	64	0.57
	60	HS{1,6} ($\beta = 10/t_p$)	100	110	90	59	0.62
		WURST (n=6)	100	160	90	63	0.63
		Chirp ($t_r = 30$ ns)	100	160	90	57	0.66
		HS{1,1} ($\beta = 6/t_p$)	100	110	90	53	0.57
33.93	100	HS{1,6} ($\beta = 10/t_p$)	100	110	100	60	0.57
		WURST (n=6)	100	160	100	63	0.62
		Chirp ($t_r = 10$ ns)	36	120	90	57	0.47
		HS{1,1} ($\beta = 6/t_p$)	100	110	90	65	0.53
	60	HS{1,6} ($\beta = 10/t_p$)	100	110	90	64	0.60
		WURST (n=6)	100	120	100	59	0.57
		Chirp ($t_r = 10$ ns)	36	120	90	58	0.47
		HS{1,1} ($\beta = 8/t_p$)	100	90	80	58	0.48

Table S10: MNR for the different broadband shaped pulses with a Gaussian observer pulse. The MNR has been evaluated up to 2 μs. The chirp pulse where no t_r time is specified is a pulse without the quartersine smoothing.

f_{obs} [GHz]	Obs. Amp. [%]	Pump pulse	t_π [ns]	Δf [MHz]	Offset [MHz]	MNR	Mod. depth λ
33.91	100	HS{1,6} ($\beta = 10/t_p$)	100	90	90	65	0.60
		WURST (n=6)	100	160	90	64	0.64
		Chirp ($t_r = 10$ ns)	36	120	80	59	0.50
		HS{1,1} ($\beta = 6/t_p$)	100	110	90	68	0.58
	60	HS{1,6} ($\beta = 8/t_p$)	100	110	90	71	0.63
		WURST (n=6)	100	160	100	67	0.63
		Chirp ($t_r = 10$ ns)	100	120	90	59	0.48
		HS{1,1} ($\beta = 6/t_p$)	100	110	90	63	0.58
33.93	100	HS{1,6} ($\beta = 10/t_p$)	100	90	90	73	0.57
		WURST (n=6)	100	160	100	72	0.62
		Chirp (no smoothing)	36	120	80	65	0.49
		HS{1,1} ($\beta = 8/t_p$)	100	110	90	71	0.52
	60	HS{1,6} ($\beta = 10/t_p$)	100	110	90	82	0.61
		WURST (n=6)	100	160	90	73	0.63
		Chirp ($t_r = 9$ ns)	36	120	80	63	0.47
		HS{1,1} ($\beta = 8/t_p$)	100	110	80	74	0.52

S16 The MNR of the diluted sample evaluated up to 7 µs

Table S11: MNR for the different broadband shaped pulses with a Gaussian observer pulse. The MNR has been evaluated up to 2 µs. The chirp pulse where no t_r time is specified is a pulse without the quartersine smoothing.

f_{obs} [GHz]	Obs. Amp. [%]	Pump pulse	t_π [ns]	Δf [MHz]	Offset [MHz]	MNR	Mod. depth λ
33.93	100	HS{1,6} ($\beta = 10/t_p$)	100	90	90	61	0.55
		WURST (n=6)	100	160	100	54	0.59
		Chirp (no smoothing)	36	120	80	58	0.46
		HS{1,1} ($\beta = 8/t_p$)	100	110	90	65	0.47
	60	HS{1,6} ($\beta = 10/t_p$)	100	110	90	59	0.56
		WURST (n=6)	100	160	90	53	0.58
		Chirp ($t_r = 9$ ns)	36	120	80	54	0.43
		HS{1,1} ($\beta = 8/t_p$)	100	110	80	55	0.46

S17 Correlation between the background density and the modulation depth

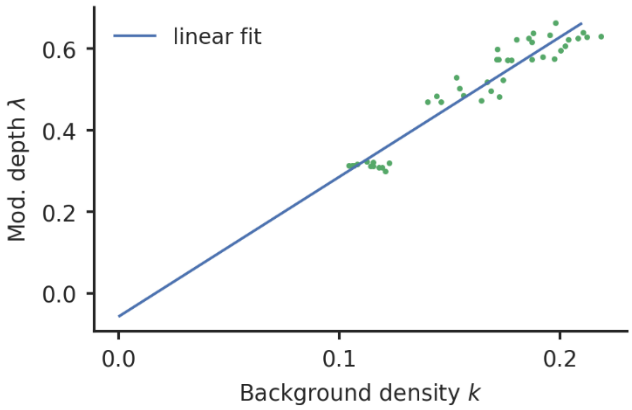

Figure S11: The correlation between the modulation depth and the background. Each dot represents a DEER trace that has been measured in the course of this study. Theoretically, the modulation depth and the background density should lie on a line through the origin. This is in fact roughly the case. The determination of the background density k seems to give a rather large error, which causes the deviations from the expected result. The fitted line has a slope of 3.43 and an x-axis distance of -0.06.

S18 Background of diluted sample with 30 µM ligand concentration

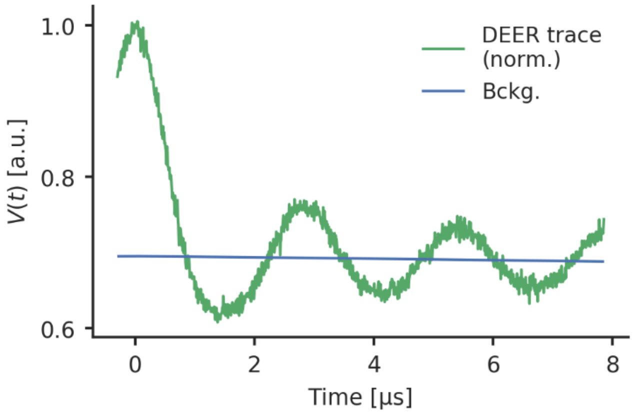

Figure S12: The (normalised) raw data of the sample with a ligand concentration of 30 µM spin concentration and rectangular pulses. It can be seen that there is almost no background decay (blue).

S19 Calculation of the background-dependent performance of broadband shaped pulses

To quantify the effect of the broadband shaped pulses on the background decay, we performed some analytical calculations. The background decay reduces the echo-intensity and therefore decreases the signal-to-noise ratio towards the end of the DEER trace. Whereas the measured trace $V(t)$ has a constant noise level σ_0, the background corrected form factor has an increasing noise level towards the end:

$$\sigma(t) = \sigma_0 \exp(kt), \tag{1}$$

where $\sigma(t)$ is the noise of the form factor and k is the background decay factor. Here, we assumed a 3D background. As discussed in the main text, the form factor is truncated at a time $t_{\text{truncation}}$ to exclude the later part. An integration from $t = 0$ to $t = \tau_{\text{truncation}}$, with $\tau_{\text{truncation}}$ as the dipolar evolution time, yields the average noise in the form factor

$$\sqrt{<\sigma^2>} = \sigma_0 \sqrt{\frac{1}{2k\tau_{\text{truncation}}}(\exp(2k\tau_2) - 1)}. \tag{2}$$

The modulation-to-noise (MNR) as the ration of the modulation depth λ and the average noise is then described by:

$$\text{MNR} = \frac{\lambda}{\sigma_0} \sqrt{\frac{2k\tau_{\text{truncation}}}{\exp(2k\tau_{\text{truncation}}) - 1}}. \tag{3}$$

As both the modulation depth λ and the background density k directly depend on the inversion efficiency, a linear dependence can be expected between them. Indeed, we experimentally found an approximately linear correlation between them (Fig. S11). Whereas the η_{2P} value captures a decrease in echo intensity it will miss the effect of a larger background decay. We chose exemplary parameters that resembled our experimental findings. For the modulation depth, we assumed an increase from 30 % to 50 %. For the density of the background we assumed an increase about the same factor: $k_\text{S} = \frac{5}{3} k_\text{R}$ with k_S as the background density for the broadband shaped pulse and k_R as the background density for the rectangular pulse. According to equation (4) this will give an MNR increase of

$$\text{MNR}_{\text{increase}} = \frac{5}{3} \sqrt{\frac{5\,(\exp(2\text{k}_\text{R}\tau_{\text{truncation}}) - 1)}{3\,(\exp(\frac{10}{3}\text{k}_\text{R}\tau_{\text{truncation}}) - 1)}}. \tag{4}$$

The heat map in Fig. S13 gives the result of this equation for different values of k_R and $\tau_\mathrm{truncation}$.

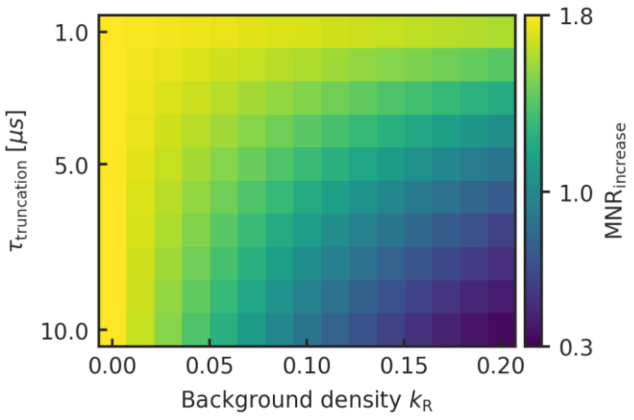

Figure S13: The MNR-ratio of adiabatic and rectangular pulses as a function of the background density (with rectangular pulses) and the $\tau_\mathrm{truncation}$-time. As the background density reflects the concentration the x-axis is a measure for the concentration of the spin centres.

Our results hint that the performance of shaped pulses can heavily depend on the circumstances of the measurement. For long traces and high concentrations, where a strong background decay has to be expected, broadband shaped pulses can further increase this decay and therefore increase the noise level. For short traces and low concentration on the other hand the increase in modulation depth due to broadband shaped pulses outperform the steeper background decay. Note that for our measurements, we typically had a k_R of about 0.1 at a concentration of 80 µM with rectangular pulses. This means that a value of 0.2 would correspond to a concentration of 160 µM which is a lot larger than what is needed for most practical applications (Jeschke, 2012). This means that in all relevant cases a sensitivity increase can be expected when broadband shaped pulses are used. Particularly, broadband shaped pulses perform better for lower concentrations and for shorter distances who allow to pick a shorter dipolar evolution time. For practical applications, a sensitivity increase due to adiabatic pulses is mostly desirable for samples with large distances and low concentrations who typically suffer the most from a low sensitivity. Our results hint that whereas for small concentrations a MNR improvement owing to broadband shaped pulses can be expected, however, this increase gets worse for longer dipolar evolution times.

S20 Comparison of the resonator profiles

Figure S14 shows the resonator profiles of the measurement of the sample with the high and the low concentration. The B_1 strengths that have been achieved for the sample with the low concentration were a bit lower.

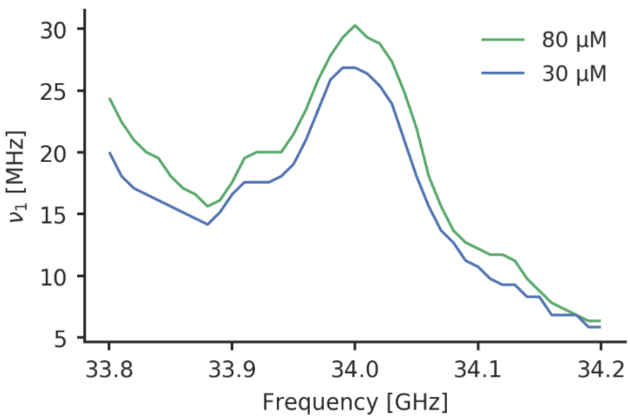

Figure S14: Resonator profiles for samples with an 80 μM concentration (green) where all optimisation measurements have been performed and for the sample with a 30 μM concentration (blue).

S21 Supporting Information References

Doll, A. and Jeschke, G.: Fourier-transform electron spin resonance with bandwidth-compensated chirp pulses, J. Magn. Reson., 246, 18–26, doi:10.1016/j.jmr.2014.06.016, 2014.

Jeschke, G.: DEER Distance Measurements on Proteins, Annu. Rev. Phys. Chem., 63(1), 419–446, doi:10.1146/annurev-physchem-032511-143716, 2012.

Stoll, S. and Schweiger, A.: EasySpin, a comprehensive software package for spectral simulation and analysis in EPR, J. Magn. Reson., 178(1), 42–55, doi:10.1016/j.jmr.2005.08.013, 2006.

Tait, C. E. and Stoll, S.: Coherent pump pulses in Double Electron Electron Resonance spectroscopy, Phys. Chem. Chem. Phys., 18(27), 18470–18485, doi:10.1039/C6CP03555H, 2016.